Weak localization effects in ZnO surface wells

A. Goldenblum, V. Bogatu, and T. Stoica
National Institute of Materials Physics, P.O. Box MG-7, Bucharest-Magurele 76900, Romania

Y. Goldstein and A. Many
Racah Institute of Physics, The Hebrew University of Jerusalem, Jerusalem 91000, Israel

(Received 15 March 1999)

Hall effect, magnetoresistance, and electrical conductivity measurements, carried out on ZnO surface wells created by a large variety of methods, are analyzed in the frame of the weak-localization theory. The ZnO surface wells have some unique features that allow the investigation of the weak-localization effects: ZnO has a single valley conduction band; the Thouless length is much larger than the elastic mean-free path even at room temperature; the well accumulates the largest surface electron concentration obtained up to now in a surface quantum well; there are a large variety of preparation methods, some of them making it possible to modify independently both the width and the depth of the surface wells. These features allowed us to investigate: the presence of the weak-localization effect in the largest range of temperatures (1.6–300 K) reported up to now for a quantum well; the influence on the transport properties of the increase in the number of subbands in the well; the effect of the presence of more inelastic scattering mechanisms and their weights in the entire scattering process; and the passage from a quasi-two-dimensional system to a three-dimensional one.
[S0163-1829(99)01932-3]

I. INTRODUCTION

The subject of electron transport and localization in a quasi-two-dimensional (2D) system is of high-scientific interest. In the past years there have been great advances in the understanding of this phenomena. A scaling theory was developed for the electronic conduction in disordered systems having various dimensionalities.[1–4] This was followed by some perturbative treatments using methods of many-body quantum theory.[5,6] One of them is based on the weak-localization concept. The weak localization is a result of the constructive interference of electron waves travelling along closed paths in opposite directions. The most spectacular consequence of this effect in a 2D system is a logarithmic dependence of the electrical conductivity on temperature.[3] However, another model that takes into account the electron-electron interaction predicts the same logarithmic dependence.[7] Nevertheless, the predictions of the two models for magnetoconductance and Hall effect appeared to be sufficiently different to distinguish between them by experiment.

Most of the experimental work carried out to verify the theoretical predictions was done on Si inversion layers at the Si-SiO_2 interface in metal-oxide-semiconductor (MOS) structures.[8–11] There are some difficulties in the interpretation of the experimental results for the Si-SiO_2 system. For example, Si has a six-valley conduction-band degeneracy. This fact creates great complications for the theoretical treatment, determined by the presence of intervalley inelastic scatterings.[12] On the other hand the interpretation of the experimental results needs using both above mentioned theories simultaneously and sometimes the interpretation is difficult.[8–10]

In this paper we will analyze a different system, the ZnO surface well. This system allows a much more accurate interpretation of the experimental data in the frame of the weak-localization theory and over a much larger range of temperatures than in the case of Si inversion layers.

There are many advantages using the ZnO system. ZnO has a single-valley conduction band so that the above-mentioned complication disappears. Extremely strong accumulation layers can be produced on ZnO surfaces. Surface electron densities up to 5×10^{14} cm^{-2} have been achieved,[13–15] i.e., about two orders of magnitude higher than those obtained in silicon inversion layers on MOS structures. These accumulation layers are characterized by a width of the order of tenths Ångstroms. The quantization effects are therefore very pronounced and the layers constitute a nearly perfect 2D electron gas system presenting a metallic conductivity. At these large electron concentrations, the screening effect is so high that the electron-electron interaction is expected to be lower than in Si inversion layers. Therefore, we can assume that the weak-localization effect will be dominant.

On the other hand, the condition for the presence of a weak-localization effect, which is that the characteristic Thouless length[3] be larger than the elastic scattering length, is fulfilled in ZnO up to room (or even higher) temperatures.

This is a remarkable peculiarity of ZnO accumulation layers. In contrast to this, in the case of Si inversion layers the weak-localization effects are evidenced only in a range of a few Kelvin degrees above absolute zero.

Another key aspect which favors the ZnO system is the possibility to modify independently the depth and the width of the surface wells. This allows the investigation of the behavior of the conductivity if more than one subband is involved in the conduction process, up to the change over to a three dimensional behavior.

In the following, experimental data (some of them reported in other contexts) concerning Hall effect, magnetoresistance and conductivity will be interpreted in the frame of the weak-localization model.

 ©1999 The American Physical Society

II. EXPERIMENT

The starting ZnO materials were Li-doped single crystals grown by Airtron Corp. and polycrystalline thin films grown by rf magnetron sputtering in our laboratories.[16] The single-crystal samples were cut in smaller chips with the hexagonal c axis perpendicular to the large surfaces. The thin film samples have also the c axis perpendicular to the surface, an orientation resulting directly from the deposition process.[16]

A large number of methods were used to produce accumulation layers on free ZnO surfaces: (1) exposure to atomic hydrogen;[17] (2) illumination of ZnO crystals in vacuum by band gap light;[18] (3) exposure to thermalized He^+ ions produced in an electrical discharge in He gas at atmospheric pressure;[19] and (4) low-energy hydrogen ion implantation.[14,15,20]

Common to the first three methods is a high sensitivity of the surface electron accumulation layer so produced to oxygen. Therefore, all measurements are made in high vacuum, *in situ*. Contrary, the strong accumulation layers produced in ZnO by hydrogen implantation are inert to oxygen and therefore their characterization is much easier. The hydrogen implantation has also the advantage that the depth and the width of the wells can be varied independently by changing the implantation dose or the energy of the hydrogen ions.

The surface wells were created on the oxygen faces of these hexagonal crystals. A large variety of contacts were realized on the surface: In dots, Vn strips, Cr-Au strips. In the majority of conductivity measurements, separate current and voltage contacts were used.

The Hall effect was usually measured between three pairs of parallel probes and we considered only those results where the difference between the pairs was less than 10% in order to avoid the inhomogenity problem. In the case of the small signal values detected in the magnetoresistance measurements, accurate data can only be obtained in the range of 10^{13}–10^{14} cm^{-2} surface electron concentration because in other ranges an understandable noise disturbs the useful signal.

The measurements were performed using a cryostat that allows conductivity and galvanomagnetic measurements to be carried out in the temperature range of 1.6–300 K. Special care was taken in order to ensure that no conductivity decay occurred during the measurement cycles due to oxygen adsorption.[13]

III. RESULTS AND ANALYSIS

A. The energy spectrum of electrons in the quantum wells

The large variety of preparation methods determines a large diversity of quantum well shapes and energy level spectra. They were calculated using the basic Hartree method, which requires a self-consistent solution of the Schrödinger and Poisson equations taking into account the specific charge distribution for each kind of structure.

For instance, in the case of samples prepared by exposing the surface to atomic hydrogen or thermalized He^+ ions, all the positive charge is fixed at the surface. Therefore the charge density that enters in the Poisson equation is only the one that corresponds to the electrons which are distributed in the accumulation layer

$$\frac{d^2V}{dx^2} = -\frac{\rho_1^-(x)}{\epsilon_0\epsilon_r}, \tag{3.1}$$

where x is the distance in the direction perpendicular to the surface, ϵ_0 is the permitivity of free space, and ϵ_r the relative dielectric constant.

In the case of hydrogen ion implantation the charge density is a sum of the positively charged donors resulting from implantation and of the negative charge determined by the electron distribution in the well

$$\frac{d^2V}{dx^2} = -\frac{1}{\epsilon_0\epsilon_r}[\rho_1^-(x)+\rho_2^+(x)], \tag{3.2}$$

where the negative charge density of electrons is

$$\rho_1^-(x) = -e\sum_{i,k}\frac{|\varphi_{ik}(x)|^2}{1+\exp\left(\frac{E_{ik}-E_F}{kT}\right)}. \tag{3.3}$$

Here φ_{ik} is the electron wave function obtained from the coupled Schrödinger-Poisson equations, E_F is the Fermi energy and E_{ik} is the energy of an electron in the ith subband

$$E_{ik} = E_{i0} + \frac{\hbar^2 k_y^2}{2m^*} + \frac{\hbar^2 k_z^2}{2m^*} = E_{i0} + \frac{\hbar^2 k^2}{2m^*}. \tag{3.4}$$

The distribution of the positive ionized donors is given by the Lindhard, Scharf, and Schiott theory and has the form of a Gaussian.[21] More details on the computation methods and about the boundary conditions can be found in another paper.[22] The shape of the potential well together with the energy levels within the well are presented in Fig. 1. We can see that for the positive charge fixed at the surface we have two subbands under the Fermi level [Fig. 1(a)]. This aspect is present for the entire range of investigated concentrations (10^{13}–10^{14} cm^{-2}). In all cases the shallow level is very close to the Fermi energy position. However, for a well obtained by 100-eV energy hydrogen implantation, having 10^{14}-cm^{-2} donor concentration, we found already three subbands [Fig. 1(b)]. The number of the levels increases up to five for 400 eV and 10^{14} cm^{-2} and even to eleven for an ion energy of 500 eV and 5×10^{14} cm^{-2} surface donor concentration [Fig. 1(c)].

The separation between the subbands has a real meaning only if it is higher than kT or ΔE-the energy broadening due to collisions. ΔE is determined from the ratio $\hbar/\tau$ where τ is the collision time. Its value can be estimated from Hall measurements (see below) and depends on the electron concentration, defect concentration, and more generally on the degree of disorder. For example, for a surface electron concentration around 10^{14} cm^{-2} the value of ΔE is about 100 meV. Therefore, we see that the upper subbands in Fig. 1(b) can be considered as being completely separated. In contrast, in the case of 500 eV and 5×10^{14} cm^{-2} electron concentration [Fig. 1(c)] the subbands seems to be superimposed each other with its neighbor levels. In this case it is expected that the system behaves like being three dimensional rather than two dimensional.

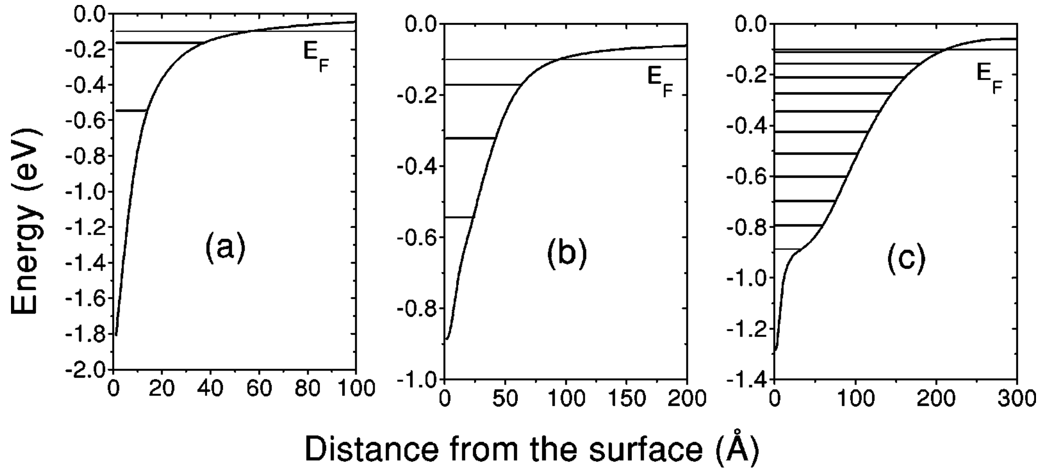

FIG. 1. The calculated shape of the surface potential and the corresponding distribution of the energy levels for three different cases. (a) Surface treated sample (i.e., all the donors at the surface) having the number of total donors per unit area equal to 6.5×10^{13} cm^{-2}; (b) hydrogen implanted sample with 100-eV ion energy having the total number of implanted donors per unit area equal to 10^{14} cm^{-2}; (c) hydrogen implanted sample with 500-eV ion energy having the total number of implanted donors per unit area equal to 5×10^{14} cm^{-2}. The position of the Fermi level in all three cases is 0.1 eV below the conduction band in the bulk.

B. The Hall effect

The Hall coefficient R_H for surface channels is usually defined as $R_H=E_H/IB$ using the value I of the current per sample width instead of the current density J as in the 3D case. Here E_H is the Hall field and B is the magnetic induction. In Fig. 2, we present the temperature dependence of the reciprocal of the Hall coefficient multiplied by the electronic charge (for reasons that will be clarified below). As can be seen from this figure the reciprocal of the Hall coefficient is essentially temperature independent in the 2–300 K range both for the helium surface-treated and the implanted samples. This behavior was typical in the metallic regime of conduction for all the investigated samples. However, some surface-treated samples show a small deviation from this constancy but only in the high-temperature range. A great number of Hall measurement data can be found in earlier published papers.[13,14]

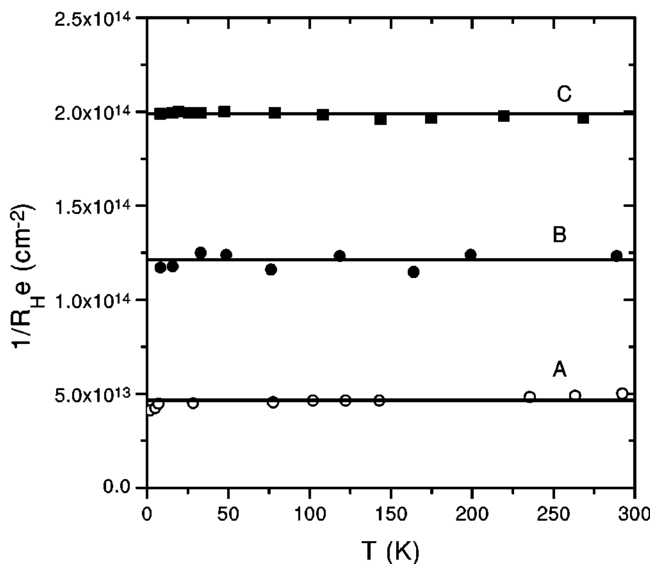

FIG. 2. The temperature dependence of the reciprocal of the surface Hall constant for three different samples. Curve A corresponds to a He treated sample, curves B and C correspond to 100-eV hydrogen-implanted samples.

The fact that in our experiments the variation with temperature of the Hall constant (ΔR_H) is zero indicates that the weak localization effects determine the transport properties of the system,[3] and not the electron-electron interaction. Indeed, in the case of electron-electron interaction the corresponding theory predicts that[23]

$$\frac{\Delta R_H}{R_H}=-2\frac{\Delta\sigma}{\sigma}, \tag{3.5}$$

which is obviously not the case here.Therefore the constancy of the Hall coefficient is a clear sign of weak localization, as shown by Fukuyama.[24] This behavior of the Hall effect allows the use of an effective surface density

$$n_{seff}=\frac{1}{eR_H}. \tag{3.6}$$

Therefore the value of $1/eR_H$ in Fig. 2 corresponds to the surface electron concentration.

Correspondingly the σ_{xx} conductivity can be written as

$$\sigma_{xx}=\frac{n_{seff}e^2}{m^*}\tau_{eff}, \tag{3.7}$$

where τ_{eff} is[24]

$$\tau_{eff}=\tau_{el}\left(1-\frac{1}{2\pi E_F\tau_{el}}\ln\frac{\tau_i}{\tau_{el}}\right). \tag{3.8}$$

Here, τ_i and τ_{el} are the inelastic and elastic collision mean times, respectively. From magnetoresistance and conductivity measurements (see below) we obtain the temperature dependence of σ_{xx} and τ_i and therefore, from Eq. (3.8) the values of τ_{el}. They were found to be between 2×10^{-15} and 9×10^{-15} s for different samples and electron concentrations.

For the same sample τ_{el} increases with n_s and for the same electron concentration its value varies from sample to sample.[13]

Knowing the value of τ_{el} we can calculate the mean-free elastic length: $l_{el}=v_{Fi}\tau_{el}$ where v_{Fi}, the velocity of an electron in the ith subband at the Fermi level, is given by

$$v_{Fi}=\left[\frac{2}{m^*}(E_i-E_F)\right]^{1/2}. \tag{3.9}$$

For example, in the case of hydrogen surface-treated samples having an electron concentration of 5×10^{13} cm^{-2} only the contribution of the deepest level is important. From the value of E_i-E_F obtained from Fig. 1(a) and the value of τ_{el} obtained from Hall measurements a value of 43 Å results for l_{el}. This is very close to the width of the well at the Fermi level [Fig. 1(a)] which suggests that the collision with the walls of the well is the main elastic scattering mechanism. However, sometimes, at high-surface electron concentration levels, the value of l_{el} can be lower than that of the width of the well.

C. Magnetoconductance

A transverse positive magnetoconductance (negative magnetorezistance) has been found for all investigated samples. This is a specific behavior of the weak-localization mechanism because the magnetic field suppresses the quantum constructive interference effect.[3,4] In contrast, the magnetoconductance determined by the electron-electron interaction is negative being isotropic for spin splitting and transverse for the orbital part.[3]

A smaller magnetoconductance was also observed in the longitudinal direction but again as a positive one. Therefore, we suppose that this longitudinal component also corresponds to a weak-localization effect being determined by the surface roughness, which allows the presence of a normal component of the magnetic field even if it is parallel to the sample surface.

Therefore, both the Hall effect and magnetoconductance measurements are in the favor of a weak-localization mechanism that is responsible for the transport phenomena in the ZnO surface well. There is a very well developed theory for magnetoconductance determined by the weak-localization mechanism in 2D systems. Thus, as Hikami, Larkin, and Nagaoka showed the change in conductivity with magnetic field (B) is given by[25]

$$\begin{aligned}\Delta\sigma&=\sigma(H,T)-\sigma(0,T)\\&=\frac{\alpha e^2}{2\pi^2\hbar}\left[\psi\left(\frac{1}{2}+\frac{\hbar}{4DeB\tau_i}\right)-\psi\left(\frac{1}{2}+\frac{\hbar}{4DeB\tau_{el}}\right)+\ln\frac{\tau_i}{\tau_{el}}\right].\end{aligned} \tag{3.10}$$

Here $\psi(Z)$ is the digamma function, D is the diffusivity and α is a coefficient that, if the spin-orbit and magnetic scatterings are weak, is equal with 1.

Since in our case, in the usual magnetic field range, $\hbar/4DeB\tau_{el}\gg1$, Eq. (3.10) becomes[25]

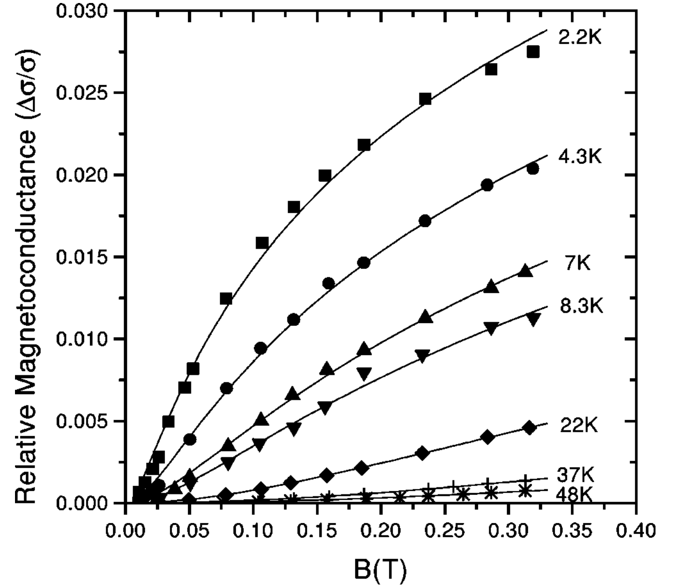

FIG. 3. The magnetic field dependence of the relative magnetoconductance (points) at different temperatures for a He-treated sample, having a surface electron concentration of 6.5×10^{13} cm^{-2}. The curves were calculated using Eq. (3.11).

$$\Delta\sigma=-\frac{\alpha e^2}{2\pi^2\hbar}\left[\ln\left(\frac{\hbar}{4DeB\tau_i}\right)-\psi\left(\frac{1}{2}+\frac{\hbar}{4DeB\tau_i}\right)\right]. \tag{3.11}$$

The magnetoconductance experimental data are shown in Fig. 3 for a He^+-treated surface sample in a large range of temperatures. Other samples with different surface electron concentrations present the same behavior.[26] The experimental data are fitted to Eq. (3.11) and an excellent agreement was found as we can see in Fig. 3.

For low-magnetic fields the expression (3.10), as Hikami shown,[25] has a very simple form

$$\Delta\sigma=\frac{\alpha e^2}{48\pi^2\hbar}\left(\frac{4DeB\tau_i}{\hbar}\right)^2. \tag{3.12}$$

Such a quadratic field dependence of $\Delta\sigma$ was evidenced in a previous article for a number of different samples and concentrations.[26]

From the fits above mentioned the parameter α and the inelastic scattering time can be extracted. The mean value of α corresponding to the curves in Fig. 3 was found to be 0.89 ±0.05. This is close to the theoretical value of 1. The resulting values of τ_i from these fits are shown in Fig. 4. It is seen that there is a large temperature range where $\tau_i\propto T^{-1}$. This corresponds to a breaking-phase-time constant determined by the inelastic electron-electron scattering.[3] This dependence was also found in many 2D systems like the inversion layer of Si (in a much lower temperature range) and thin films of In_2O_3,[27] PdC,[28] NiSi.[29]

D. Electrical conductivity

Following the single-parameter scaling theory developed by Abrahams *et al.*,[2] in the high-conductivity limit the scaling length (L) dependence of the conductivity of a 2D electron gas is given by

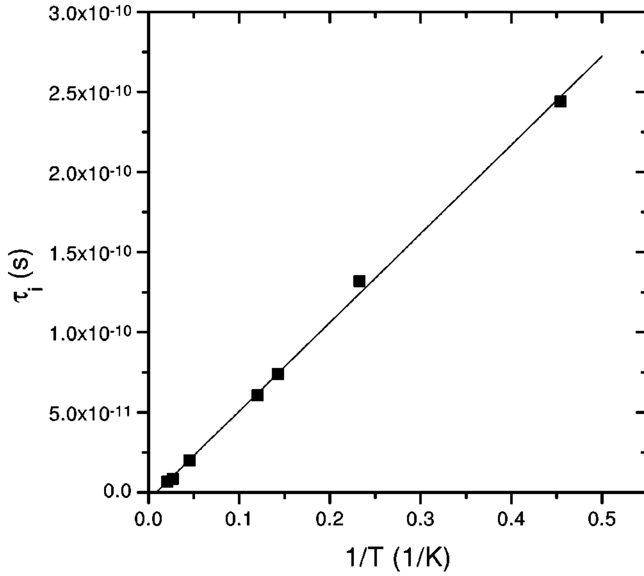

FIG. 4. The temperature dependence of the inelastic scattering time derived from the fit between the experimental points in Fig. 3 and Eq. (3.11).

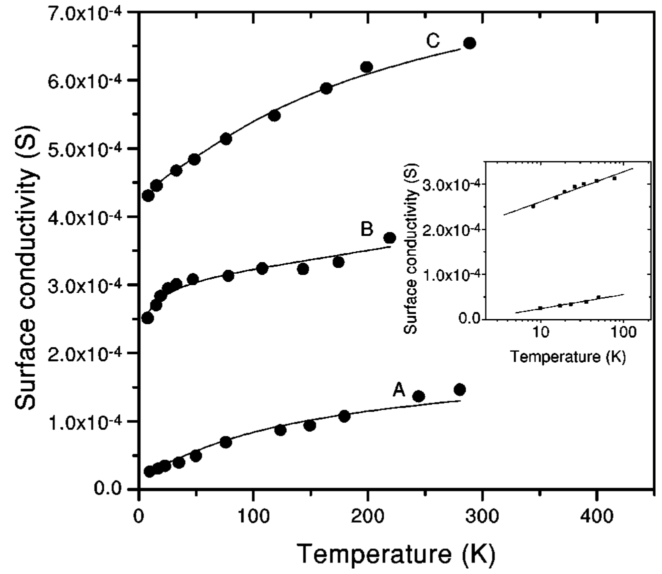

FIG. 5. The surface conductivity versus temperature for three different samples: curve A corresponds to a hydrogen surface-treated sample having an electron concentration of 4×10^{13} cm^{-2}; curve B corresponds to a 100-eV hydrogen-implanted sample having a surface electron concentration of 2×10^{14} cm^{-2}; curve C corresponds to a 100-eV hydrogen-implanted sample having a surface electron concentration of 1.25×10^{14} cm^{-2}. The curves result from the fit between experimental points and Eq. (3.22). The inset shows the temperature dependence of the surface conductivity in a semi-logarithmical representation, in the lower range of temperatures, for the samples A and B.

$$\sigma(L)=\sigma_0-\frac{\alpha e^2}{\pi^2\hbar}\ln\left(\frac{L}{l_{el}}\right). \tag{3.13}$$

In the case of a weak-localization mechanism the cutoff scaling length is the Thouless length (L_{Th}) determined by a specific inelastic mechanism

$$L_{Th}=(D\tau_i)^{1/2}. \tag{3.14}$$

Therefore, the conductivity is given by

$$\sigma(L)=\sigma_0'-\frac{\alpha e^2}{2\pi^2\hbar}\ln\tau_i, \tag{3.15}$$

where in σ_0' are included all the remaining terms. We found from magnetoconductance measurements that in our samples, at relatively low temperatures, τ_i depends on the temperature as

$$\tau_i\propto T^{-1}, \tag{3.16}$$

and therefore,

$$\sigma(L)=\sigma_0''+\frac{\alpha e^2}{2\pi^2\hbar}\ln T. \tag{3.17}$$

Again σ_0'' includes the remaining terms.

The inset of Fig. 5 shows that indeed this logarithmic dependence on temperature is present in our structures. From this fit the value of the parameter α is found to be 0.93 ±0.1 for the lower curve (corresponding to a hydrogen surface-treated sample) and 2.0 ± 0.1 for the upper curve (corresponding to a hydrogen-implanted sample). The first value is very close to the ideal 2D system value of 1. The difference between the values of the logarithmic term prefactor corresponding to the two structures is due to the difference in the energy spectrum of the two corresponding wells. As we can see in Fig. 1(a) if the donors are concentrated at the surface, like in the hydrogen-treated samples, there are two subbands. However, in the upper band closer to the Fermi level, the wave vector k_F of the electrons at the Fermi level has a low value. Therefore, the Ioffe-Regel criterion for a metallic conduction ($k_Fl_{el}>1$) is not fulfilled for this subband. Thus, in this case only the lower level contributes to the metallic conduction. This corresponds to the case of an ideal 2D system, having $\alpha=1$.

On the other hand, in the case of a 100-eV implanted sample there are three (or more) subbands. However, similarly to the previous case, only the lowest two subbands are involved in the metallic conduction of the system. The problem of weak localization in systems having two occupied subbands was treated recently by Averkiev, Golub, and Pikus.[30] They show that if we deal with a long-range scattering potential and at the same time the interband scattering time is much larger than the breaking phase time then both subbands give independent contributions to the conductivity. In our case, it is expected that the dominant scattering mechanism in the implanted sample having high-donor concentration will be on charged centers. This corresponds to a long-range Coulomb scattering potential and therefore, the Eq. 2.24 from Ref. 3 can be integrated for each subband with the corresponding L_{Th1} and L_{Th2} upper cutoff lengths to obtain

$$\sigma(L)=\sigma_0-\frac{\alpha e^2}{\pi^2\hbar}\ln\left(\frac{L_{Th1}}{l_{el1}}\right)-\frac{\alpha e^2}{\pi^2\hbar}\ln\left(\frac{L_{Th2}}{l_{el2}}\right). \tag{3.18}$$

If the subbands are deep enough then the same inelastic scattering mechanism is involved for electrons in both subbands

TABLE I. The values of some parameters of the samples corresponding to Figs. 5 and 6. The first number in the column labeled ''Sample'' is the figure number and the letter refers to the curve in the relevant figure.

Sample	System	Surface concentration (cm^{-2})	b_2 or b_3 value
5-*A*	2D	4×10^{13}	1.45×10^{-5}
5-*C*	2D	1.25×10^{14}	3.9×10^{-6}
5-*B*	2D	2×10^{14}	8.7×10^{-8}
6-*A*	3D	1.2×10^{14}	2.15×10^{-5}
6-*B*	3D	3.5×10^{14}	1.3×10^{-5}
6-*C*	3D	5×10^{14}	3.3×10^{-7}

and the same temperature dependence [see Eqs. (3.14), (3.16)] for the cutoff inelastic lengths results and

$$\sigma(L)=\sigma_0''+\frac{2\alpha e^2}{2\pi^2\hbar}\ln T, \tag{3.19}$$

i.e., the ideal value of α must be multiplied by 2.

The center part of Fig. 5 shows the conductivity behavior for a large temperature range. In this case, the simple law (3.17) is not adequate for describing the behavior of the curves over the entire temperature range. It is expected that at high temperatures the electron-phonon inelastic scattering will have an important effect. Therefore, when dealing with a large temperature range, one must take into account both inelastic scatterings

$$\frac{1}{\tau_i}=\frac{1}{\tau_{ie\text{-}e}}+\frac{1}{\tau_{ie\text{-}ph}}. \tag{3.20}$$

For electron-phonon scattering in disordered systems, only the qualitative temperature dependence of the inelastic scattering time, deduced by Schmid is known[31]

$$\frac{1}{\tau_{ie\text{-}ph}}\propto T^4. \tag{3.21}$$

Therefore, the conductivity in this case will have a temperature dependence of the form

$$\sigma(L)=\sigma_0''+\frac{\alpha e^2}{2\pi^2\hbar}\ln(T+b_2T^4), \tag{3.22}$$

where b_2 is a constant related to the weight of the electron-phonon inelastic scattering process relative to the electron-electron inelastic scattering process.

A good fit between the experimental points and the theoretical prediction (3.22) is obtained for the data in Fig. 5, over the entire temperature range. The values of b_2 resulting from this fit are given in Table I. For all investigated samples the constant prefactor of the logarithmic term in $e^2/2\pi^2\hbar$ units, is around 1 for the surface-treated structures and about 2 for the 100-eV implanted structures. As we have already shown, by changing the dose and the ion implantation energy we can widen or deepen the wells so that the system becomes a three-dimensional one. The transition from a two-dimensional system to a three-dimensional one manifests itself as a change in the curvature of the temperature dependence of the conductivity from a convex to a concave shape (Figs. 5 and 6).

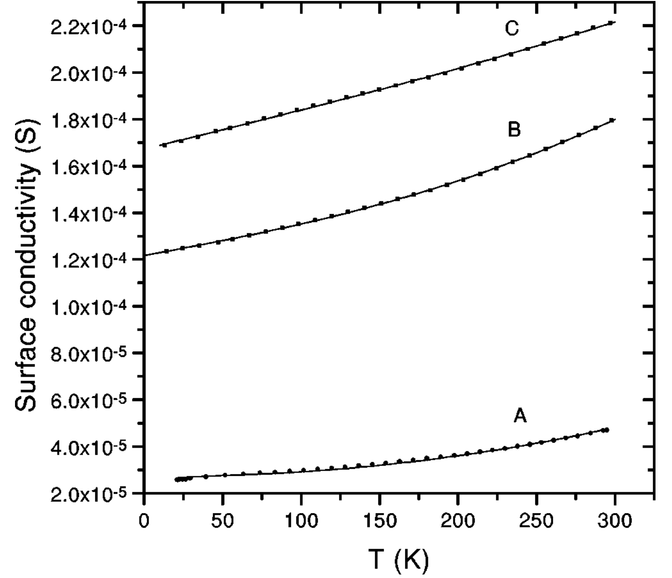

FIG. 6. Surface conductivity versus temperature for three different 500-eV hydrogen-implanted samples having surface electron concentrations of 1.2×10^{14} cm^{-2} for sample *A*, 3.5×10^{14} cm^{-2} for sample *B* and 5×10^{14} cm^{-2} for sample *C*.

For a 3D system the scaling theory predicts for the conductivity

$$\sigma_{3D}(L)=\sigma_0-\frac{e^2}{\hbar\pi^3}\left(\frac{1}{l_{el}}-\frac{1}{L}\right). \tag{3.23}$$

In the case of a single inelastic mechanism,

$$L_{Th}\propto AT^{-p/2} \tag{3.24}$$

(p being an integer specific for each inelastic scattering mechanism) and the conductivity has a power-law dependence on temperature[3]

$$\sigma(T)=\sigma_0'+\frac{e^2}{\hbar\pi^3}\frac{1}{A}T^{p/2}. \tag{3.25}$$

Using Eq. (3.23) and the fact that in the case of the 3D systems $\tau_{ie\text{-}e}=AT^{-2}$ (the Baber formula)[32] we obtain by means of Eqs. (3.14) and (3.20)], over a large range of temperatures

$$\sigma(T)=\sigma_0'+c\sqrt{T^2+b_3T^4}, \tag{3.26}$$

where in c we included all the temperature independent terms and b_3 has a similar meaning as b_2 in Eq. (3.22). The fit between the experimental data in Fig. 6 and Eq. (3.26) is very good. The values of the parameter b_3 are also given in Table I.

One of the most interesting aspects which can be deduced from the fits in Figs. 5 and 6 is the determination of the weight of different inelastic processes involved in the conductivity. Unfortunately, the value of b varies from sample to sample and also with the electron concentration in the well.

However, a general trend can be observed and this is seen even in Table I: the value of b decreases with the increase of the surface electron concentration for both 2D and 3D systems. In the particular case of the upper curve in Fig. 6 this aspect can be directly observed since the curve is nearly linear, i.e., the contribution of the T^4 term is relatively small. This aspect was also observed in other 3D disordered systems like NiSi.[33,34] A possible explanation can be found in the diagrammatic analysis made by Schmid for the electron-phonon processes in disordered systems in the presence of impurities. He found, unfortunately only in a qualitative manner, that the time between inelastic collisions with phonons increases if impurities are added to the system. In our case, the increase of the surface electron concentration is determined by the increase of the donor concentration. This, in turn, leads to the decrease of the electron-phonon scattering rate (increase of the $\tau_{ie\text{-}ph}$ as was shown by Schmid[31]). Simultaneously, the increase of the filling level leads to a decrease also of the electron-electron scattering probability.[10] Our experimental results suggest that the decrease of the electron-electron scattering is smaller than the electron-phonon one.

ACKNOWLEDGMENTS

We are grateful to our colleague Dr. A. Manolescu for many enlighting discussions as well as to Dr. M. Suhrke of Regensburg University for carefully reading the manuscript and for helpful suggestions.

[1] D. J. Thouless, Phys. Rep. **13**, 93 (1974).
[2] E. Abrahams, P.W. Anderson, D.C. Licciardello, and T.V. Ramakrishnan, Phys. Rev. Lett. **42**, 673 (1979).
[3] P.A. Lee and T.V. Ramakrishnan, Rev. Mod. Phys. **57**, 287 (1985).
[4] B. Kramer and A. MacKinnon, Rep. Prog. Phys. **56**, 1470 (1993).
[5] P.W. Anderson, E. Abrahams, and T.V. Ramakrishnan, Phys. Rev. Lett. **43**, 718 (1979).
[6] L.P. Gor'kov, A.I. Larkin, and D.E. Khmel'nitskii, Zh. Éksp. Teor. Fiz. Pis'ma Red. **30**, 248 (1979) [JETP Lett. **30**, 248 (1979)].
[7] B.L. Altshuler and A.G. Aronov, Solid State Commun. **39**, 115 (1979).
[8] M.J. Uren, R.A. Davies, and M. Pepper, J. Phys. C **13**, L985 (1980).
[9] R.G. Wheeler, Phys. Rev. B **24**, 4645 (1981).
[10] D.J. Bishop, R.C. Dynes, and D.C. Tsui, Phys. Rev. B **26**, 773 (1982).
[11] D.J. Bishop, R.C. Dynes, B.J. Lin, and D.C. Tsui, Phys. Rev. B **30**, 3539 (1984).
[12] H. Fukuyama, Surf. Sci. **113**, 489 (1982).
[13] Y. Grinshpan, M. Nitzan, and Y. Goldstein, Phys. Rev. B **19**, 1098 (1979).
[14] G. Yaron, A. Many, and Y. Goldstein, J. Appl. Phys. **58**, 3508 (1985).
[15] G. Yaron, Y. Goldstein, and A. Many, Solid State Phenom. **1&2**, 429 (1988).
[16] A. Goldenblum, A. Oprea, and V. Bogatu, Rom. J. Phys. **41**, 679 (1996).
[17] Y. Shapira and D. Lichtman, J. Vac. Sci. Technol. **13**, 615 (1976).
[18] A. Many, Crit. Rev. Solid State Sci. **4**, 515 (1974).
[19] Y. Goldstein, A. Many, D. Eger, Y. Grinshpan, G. Yaron, and M. Nitzan, Phys. Lett. **62A**, 57 (1977).
[20] V. Bogatu, A. Goldenblum, and B. Logofatu, in *CHS '97 Proceedings*, 1997 International Semiconductor Conference, Sinaia, Romania, 20th ed. (IEEE, Piscataway, NJ, 1997).
[21] J. Lindhart, M. Scharff, and H.E. Schiott, K. Dan. Vidensk. Selsk. Mat. Fys. Medd. **33** (14) (1963).
[22] V. Bogatu, A. Goldenblum, A. Many, and Y. Goldstein, Phys. Status Solidi B **212**, 89 (1999); **212**, 397 (1999).
[23] B.L. Altshuler, D. Khmel'nitzkii, A.I. Larkin, and P.A. Lee, Phys. Rev. B **22**, 5142 (1980).
[24] H. Fukuyama, J. Phys. Soc. Jpn. **49**, 644 (1980).
[25] S. Hikami, A.I. Larkin, and Y. Nagaoka, Prog. Theor. Phys. **63**, 707 (1980).
[26] Y. Goldstein, Y. Grinshpan, and A. Many, Phys. Rev. B **19**, 2256 (1979).
[27] Z. Ovadyahu and Y. Imry, Phys. Rev. B **24**, 7439 (1981).
[28] A. Carl, G. Dumpich, and D. Hallfarth, Phys. Rev. B **39**, 3015 (1989).
[29] K.M. Abkemeier, C.J. Adkins, R. Asal, and E.A. Davis, J. Phys.: Condens. Matter **4**, 9113 (1992).
[30] N.S. Averkiev, L.E. Golub, and G.E. Pikus, Fiz. Tekh. Poluprovodn. **32**, 1219 (1998) [Sov. Phys. Semicond. **32**, 1087 (1998)].
[31] A. Schmid, Z. Phys. **259**, 421 (1973).
[32] W.G. Baber, Proc. R. Soc. London Ser. A **158**, 383 (1937).
[33] R. Rosenbaum, A. Heines, A. Palevski, M. Karpovski, A. Gladkikh, M. Pilosof, A.J. Daneshvar, M.R. Graham, T. Wright, J.T. Nicholls, C.J. Adkins, M. Witcomb, V. Prozesky, W. Przybylowicz, and R. Pretorius, J. Phys.: Condens. Matter **9**, 5395 (1997).
[34] A. Belu Marian, M.D. Serbanescu, R. Manaila, E. Ivanov, O. Malis, A. Devenyi, Thin Solid Films **259**, 105 (1995).